Effect of noble metal addition over active Ru/TiO₂ catalyst for CO selective methanation from H₂ rich-streams

L.F. Bobadilla[*], A. Muñoz-Murillo, J. Gándara-Loe, A. Pérez [1],
O.H. Laguna [2], L.M. Martínez T, A. Penkova, M.A. Centeno, J.A. Odriozola

Departamento de Química Inorgánica e Instituto de Ciencia de Materiales de Sevilla (ICMS), Centro Mixto CSIC-Universidad de Sevilla, Calle Américo Vespucio 49, 41092 Seville, Spain

HIGHLIGHTS

- Selective bimetallic catalysts for CO methanation were synthesized.
- Rh and Pt modify the electronic properties of Ru.
- RuRh catalyst is promising for the treatment of industrial-volume streams.

GRAPHICAL ABSTRACT
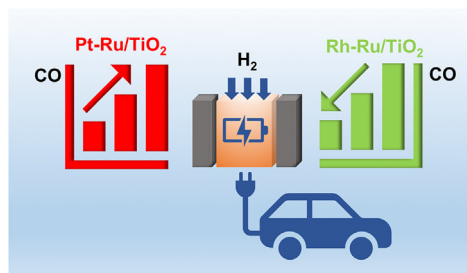
ARTICLE INFO

ABSTRACT

Selective CO methanation from H₂-rich stream has been regarded as a promising route for deep removal of low CO concentration and catalytic hydrogen purification processes. This work is focused on the development of more efficient catalysts applied in practical conditions. For this purpose, we prepared a series of catalysts based on Ru supported over titania and promoted with small amounts of Rh and Pt. Characterization details revealed that Rh and Pt modify the electronic properties of Ru. The results of catalytic activity showed that Pt has a negative effect since it promotes the reverse water gas shift reaction decreasing the selectivity of methanation but Rh increases remarkably the activity and selectivity of CO methanation. The obtained results suggest that RuRh-based catalyst could become important for the treatment of industrial-volume streams.

* *Corresponding author.*
  E-mail address: lbobadilla@us.es (L.F. Bobadilla).
  [1] Current address: Línea de Investigación en Tecnología Ambiental y de Materiales (ITAM), Departamento de Química, Facultad de Ciencias, Pontificia Universidad Javeriana, Carrera 7 No. 43-82, Bogotá D.C., Colombia.
  [2] Current address: Department of Physical Chemistry, University of Granada, Cartuja Campus, 18071 Granada (Spain).
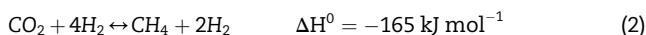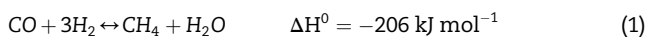
Introduction

In the last decades, hydrogen fuel cell technology has become an alternative to energy production systems in fixed and mobile devices [1]. The polymer-electrolyte-membranes fuel cells (PEMFCs) has turned into the most hopeful energy converters due to their high efficiency, no pollution, and energy suitability. Nowadays, H_2 is produced mainly by hydrocarbons steam reforming, which inherently includes a large CO concentration (0.5%–10%) in the H_2 stream [2]. However, high purity hydrogen is necessary since Pt anodes are very sensitive to impurities such as carbon monoxide and sulfides [2,3]. The CO presents a poisoning effect since it is adsorbed much easier than hydrogen on the surface of the Pt anode. Furthermore, CO is difficult to be eliminated from the active sites [4,5].

Different strategies such as pressure swing adsorption (PSA), membrane separation, water-gas shift (WGS) reaction, selective methanation, and preferential oxidation have been proposed to minimize and remove the CO concentrations in H_2 streams [2]. Among them, selective methanation of carbon monoxide (S-MET) where CO reacts preferentially to form CH_4 without CO_2 conversion, has been reported as a promissory strategy in hydrogen purification (Eqs. (1) and (2)) [6,7]:

$$CO + 3H_2 \leftrightarrow CH_4 + H_2O \qquad \Delta H^0 = -206 \, \text{kJ mol}^{-1} \qquad (1)$$

$$CO_2 + 4H_2 \leftrightarrow CH_4 + 2H_2 \qquad \Delta H^0 = -165 \, \text{kJ mol}^{-1} \qquad (2)$$

In this sense, most of the catalysts studied in this reaction can be classified as Ni- or Ru-based catalysts [8,9]. The role of the support materials and the promoters in nickel (Ni) and ruthenium (Ru) catalysts have proved to play an essential part in the enhancement of the selectivity of CO due to their direct relationship to the electron density that inherently influences the activity of CO methanation [10–13]. Due to this, if the electron density is enhanced, CO adsorbed on the metal surface is more easily dissociated by enhanced $d\pi$-$p\pi^*$ back bonding and by consequence, CO methanation is improved [14,15]. In addition, it has been reported that in Ru-based catalyst, the CO methanation activity has been improved using supports such as TiO_2 compared to others such as Al_2O_3, CeO_2, YSZ, SiO_2, ZrO_2, and MgO due to the synergy between the support and the electron density of the active phase [16,17]. Indeed, Tada and Kikuchi described a mechanistic study over Ru/TiO$_2$ catalyst for selective carbon monoxide methanation where the control of the interfaces between active metals and support materials was observed to be a key step. Due to this, the choice of suitable support materials such as TiO_2 and promoters are necessary to improve CO methanation [11].

The addition of small amounts of metals in Ru-based catalysts has been reported as a strategy to enhance the selectivity in the hydrogenation of C–O towards C–C bonding through the combination of electropositive metals giving place to particles with improved redox properties [18]. This improvement can be explained in two pathways: (i) the most electropositive metal acts as a Lewis base that increases the density in the other one, therefore decreasing the bond energy of the adsorbed species, in particular, the C–C bond, and favouring the C–O hydrogenation towards the C–C one [19]; (ii) the metal active phase act as electrophilic or Lewis acid sites for CO adsorption and activation of C–O bond through the oxygen lone pair of electrons.

Among the different metal promoters, rhodium (Rh) has proved to enhance catalytic activity in different reactions due to its ability to form solid solutions in a Ru matrix [20–22]. Additionally, Rh possess one extra electron in its electronic configuration, which can increase the electronic density to the active sites, therefore making the C–O bonding breakage becomes easier due to the back-bonding effect in the adsorbed metal. In a similar route, Platinum (Pt) is also able to form alloys with Ru, adopting an *hcp* structure at high Pt concentrations (>80%), that is, when forming solid solution Pt-Ru [23]. Pt possesses even more electronic density than Rh, which facilitates the breakage of adsorbed CO in comparison with Rh. Both Rh and Pt have intrinsic properties as methanation catalysts [24].

According to these premises, in this work we synthesize a series of active Ru/TiO$_2$ catalysts promoted with Rh and Pt to evaluate the effect of small amounts of these metals in the catalytic performance in the S-MET reaction using a real composition H_2 stream to simulate the streams outlines from the WGS and PROX units.

Experimental details

Catalysis synthesis

Ru/TiO$_2$ parent catalyst was prepared by wet impregnation method based on a similar procedure as reported elsewhere [25]. Typically, 13.2 g of nitrosyl nitrate solution (14.391 wt% of Ru, Johnson Matthey) were mixed in the necessary amount of water to impregnate 19 g of Aeroxide® TiO$_2$ P25 (Evonik) support to obtain a nominal loading of 9.5 wt% of Ru. The solid catalyst was dried at 130 °C for 24 h and finally calcined at 400 °C for 2 h.

Analogously, the bimetallic catalysts were prepared by co-impregnation of both ruthenium and platinum or rhodium precursors in order to achieve a nominal loading value of 9.5 wt% of Ru and 0.5 wt% of Pt or Rh. $Rh(NO_3)_3$ from Alfa Aesar and $Pt(NH_3)_4(NO_3)_2$ from Johnson Matthey were employed as metallic precursors. The fresh Rh-based catalyst was then calcined at 400 °C for 2 h while Pt-based catalyst was calcined at 350 °C for 8 h based on previous results of calcination conditions reported in the literature [26,27]. For clarity, the catalysts were designated as Ru–TiO$_2$, RhRu–TiO$_2$ and PtRu–TiO$_2$.

Characterization techniques

The structural analysis of the synthesized catalysts was elucidated by powder X-ray diffraction on an X-Pert Pro PANalytical (Malvern PANalytical Ltd, Malvern, UK). X-ray diffraction patterns were collected using Cu Kα as a radiation source in the range of $2\theta = 10°–80°$ with a step size of 0.05° and a step time of 80 s.

The quantitative analysis of the metal loading was performed using X-Ray Fluorescence in an Axios low-power (1 kW) wavelength dispersive XRF (WDXRF) spectrometer equipped with a Rh cathode.

The textural properties of the catalyst were evaluated using N_2 adsorption isotherms at 77 K in a Micromeritics ASAP 2010 instrument. Previous to analysis, the samples were outgassed under dynamic vacuum at 250 °C for 2 h to eliminate adsorbed molecules and impurities. The specific surface area of each solid was determined according to using the BET method. Pore volumes were determined by BJH desorption method.

Hydrogen temperature-programmed reduction (H_2-TPR) experiments were carried out placing the catalyst (0.1 g) in a U-shape quartz tube reactor and initially pretreated at 300 °C (rate 10 °C min^{-1}) in Ar atmosphere for 1 h to remove adsorbed water and then cooled to 75 °C in Ar followed by heating to 700 °C at a heating rate of 10 °C min^{-1} in a flow of 10% H_2/Ar. A thermal conductivity detector (TCD) was used to quantify the H_2 consumption. By using the same experimental set-up, the metallic particles average size distribution was determined through hydrogen chemisorption (H_2-TPD) experiments. Prior to the analysis, the samples were heated up to 300 °C under Ar flow for 45 min and then cooled down to 75 °C. Finally, the adsorption of H_2 took place and then Ar was introduced to perform the TPD measurements with a temperature ramp of 10 °C min^{-1} to 300 °C. The dispersion of Ru (D) was calculated based on the volume of chemisorbed H_2 using the following simplified equation (Eq. (3)):

$$D(\%) = 100 \left(\frac{V_{STP} \cdot S_i}{22414} \right) \left(\frac{F_i}{PM_i} \right)^{-1} \qquad (3)$$

where V_{STP} denotes the total volume of H_2 consumed (mL g^{-1}), S_i is the stochiometric factor of H_2 to Ru, which is considered $S_i = 2$ as previously reported in the literature [28,29], PM_i is the molecular weight of the active phase (mmol g^{-1}) and F_i corresponds to the fraction of active phase per gram of sample. Finally, the crystallite size was estimated using the equation (Eq. (4)):

$$d_i = \frac{6 \cdot V_i}{D \cdot a_i} \qquad (4)$$

assuming the geometry of Ru particles as hemispherical, where V_i is the average volume of a metallic bulk particle and a_i is the exposed area of a metallic atom in the surface. For the calculation, a_i for ruthenium particles was considered as a_{Ru} = 9.09 × 10^{-2} nm^3 instead of 6.29 × 10^{-2} nm^3 based on the previous work reported by Shen et al. that considered that metallic Ru is able to expose indistinctly (100), (001) and (110) planes due to their similar superficial energy [28].

X-ray Photoelectron Spectroscopy (XPS) analysis was carried out using a LEYBOLD-HEREUS model LHS-10/20 device equipped with Al-Kα radiation (1486.6 eV) and a twin crystal monochromator to produce a focused X-ray spot at 30 mA × 11 kV (400 μm major axis length of the elliptical shape). The alpha hemispherical analyzer was operated at the constant energy mode with survey scan pass energies of 200 eV to measure the whole energy band and 50 eV in a narrow scan to selectively measure specific elements. The reference binding energy was the C 1s core level at 284.6 eV.

Catalytic activity tests

The catalytic activity was measured in a continuous flow fixed-bed stainless steel reactor (i.d. 9 mm) coupled to a Microactivity Reference Unit (PID Eng&Tech®). For each experiment, 150 mg of sieved catalyst (100–200 μm) was mixed with commercial SiC (125 μm − VWR Prolabo®) up to a volume bed of 0.32 cm^3. Prior to the reaction, the catalyst was activated in pure H_2 flow of 60 mL min^{-1} at 300 °C for 1 h and subsequent cooled up to reaction temperature. The reaction was conducted at atmospheric pressure increasing the temperature from 180 °C to 300 °C with heating rate of 10 °C min^{-1}. A simulated mixture of real reformate stream containing H_2 (50%), CO_2 (15%), H_2O (15%) and CO (1% or 300 ppm) balanced with N_2 was fed at flow rate of 200 mL min^{-1} (WHSV = 80 L g^{-1} h^{-1}). The effluents were on-line analyzed in a gas micro-chromatograph Varian 4900. The CO_2 amount at the outlet was determined by a CO_2 detector Vaisala CARBO-CAP GMT220. The conversion (X_i) and selectivity (S_i) values were estimated according to the following equations (Eq. (5) to Eq. (7)):

$$X_{CO}(\%) = \frac{(F_{CO\ in} - F_{CO\ out})}{F_{CO\ in}} * 100 \qquad (5)$$

$$X_{CO_2}(\%) = \frac{(F_{CO_2\ in} - F_{CO_2\ out})}{F_{CO_2\ in}} * 100 \qquad (6)$$

$$S_{CO\ methanation}(\%) = \left(\frac{X_{CO} \cdot F_{COin}}{F_{CH_4\ out}} \right) \cdot 100 \qquad (7)$$

being F_{CO}, F_{CO_2} and F_{CH_4} the flow in mL min^{-1} of CO, CO_2 and CH_4, respectively, at the inlet (in) or the outlet (out) flow. $C_{i,\ out}$ corresponds to the concentration of product i in the outlet and v_i is the carbon number according to its chemical formula.

In all cases, the methane selectivity estimated from Eq. (8) was higher than 95% and only small traces of ethane and ethylene were detected. The carbon balance resulted to be better than 97%.

$$S_{CH_4}(\%) = \left(\frac{C_{CH_4\ out} / v_{CH_4}}{\sum_i C_{i\ out} / v_i} \right) \cdot 100 \qquad (8)$$

$C_{i\ out}$ is the product i concentration in the outlet and v_i is the carbon numbers according to its chemical formula.

Results and discussion

Physicochemical properties

Table 1 includes the wt.% metal loading values obtained by XRF analysis. As can be observed, the measured metal contents were close to the nominal values confirming that the synthesis method was successful. However, it is noticeable that Ru loading was slightly lower than that of expected one in the bimetallic catalysts. Although these differences in Ru content may seem significant, this variation can be assumed with the uncertainty of the measurement, where variations between 0.5 and 1 wt% have been reported [30].

Table 1 – Average crystalline size and textural properties of Ru-based catalysts.

Sample	Ru wt.%	Pt wt.%	Rh wt.%	Crystallite size Ru^0 (nm)[a]	S_{BET} ($m^2\,g^{-1}$)	V_{pore} ($cm^3\,g^{-1}$)	Max. $\varnothing_{pore}$(nm)
Ru–TiO$_2$	9.6			7.1	42	0.25	44
RhRu–TiO$_2$	8.3		0.54	7.6	42	0.30	85
PtRu–TiO$_2$	7.6	0.75		7.6	38	0.28	76

[a] Calculated with (101) plane.

Fig. 1a shows the XRD patterns of the as-synthesized catalysts in which are observed the typical diffraction lines of anatase (JCPDS 73-1764) and rutile (JCPDS 78-1510) phases present in the P25 titania support. Additionally, diffraction peaks ascribed to RuO$_2$ (JCPDS 21-1172) are observed in all Ru-loaded patterns. However, after the incorporation of Rh and Pt in the Ru-loaded catalysts, no additional peaks were observed in the XRD patterns possibly due to the small amount of metal added to the catalyst but also possibly due to the high dispersion of the metal. Similarly, the XRD diffraction measurements were performed in the catalyst after a reduction process in H$_2$ atmosphere to evaluate the structural changes taking place due to the reduction of the metals. Fig. 1b presents the XRD patterns of the reduced samples where the diffraction peaks related to the metallic Ru reflection planes (100), (002) and (101) are observed close to ca. $2\theta = 41.4°$, $43.7°$ and $44.1°$, which confirms the complete reduction of RuO$_2$ at the evaluation conditions. However, the diffraction peaks related to the dopant metals are not present in the patterns mostly attributed to the high dispersion of those species. The Ru metal average crystal size of the three reduced catalysts was calculated using the Debye-Scherrer method. As

summarized in Table 1, it is observed a slight increase in the crystal size in Ru-based catalyst after the incorporation of the Rh and Pt promoters which may be attributed to the interactions Ru–Pt and Ru–Rh able to form bimetallic alloys.

The textural properties of the catalyst were evaluated through nitrogen adsorption-desorption isotherms at $-196\,°C$ as displayed in Fig. 2a. It can be observed that all the isotherms present a *type III* shape according to the IUPAC classification, which is mainly attributed to non-porous or macroporous materials and hysteresis loop *type H3* usually found in materials with a wide distribution of pore size [31]. The specific surface area and pore volume of the catalysts were calculated using the BET model and D-R model, respectively. As depicted in Table 1, the incorporation of the second metal does not promote any change in the surface area, which may confirm the high dispersion of the active phase in all catalysts. Additionally, the pore volume all catalyst remains similar. However, in the bimetallic catalysts, it is observed an increase in the average particle size as a result of the possible formation of alloys [32]. The pore distribution calculated using the BJH method is shown in Fig. 2b, where a similar distribution is observed among the monometallic catalyst and the bimetallic Rh and Pt bimetallic catalysts showing a narrower pore distribution with a maximum displaced to bigger pore diameter as an effect of alloys formation.

The hydrogen consumption profiles obtained in the H$_2$-TPR measurements for all the as-synthesized catalysts are shown in Fig. 3. In general terms, the ruthenium oxide reduction can be represented by Eq. (9):

$$RuO_x + xH_2 \rightarrow Ru^0 + xH_2O \tag{9}$$

where x identifies the possible different ruthenium oxides that may be present in the sample. If we assume that the oxidation state of Ru is $+4$ for the determination of the reducibility degree, the Eq. (10) indicates that to reduce 1 mol of ruthenium oxide, 2 mol of H$_2$ are required.

$$RuO_2 + 2H_2 \rightarrow Ru^0 + 2H_2O \tag{10}$$

Based on previous results reported in the literature related to Ru/TiO$_2$, these types of catalysts show three TPR signals in their profiles attributed to three different reduction zones [33,34]. The signal at lowest temperature (approximately at 105 °C) has been established to be related to RuO$_x$ well dispersed amorphous species. The second reduction zone, at approximately 125 °C, is attributed to the RuO$_x$ species within the bulk. Finally, the peak at 150 °C was attributed to the reduction of the RuO$_x$ species strongly interacting with the support, being these ones the hardest to be reduced.

All the catalysts present the typical reduction profiles described above. However, the bimetallic catalysts present an
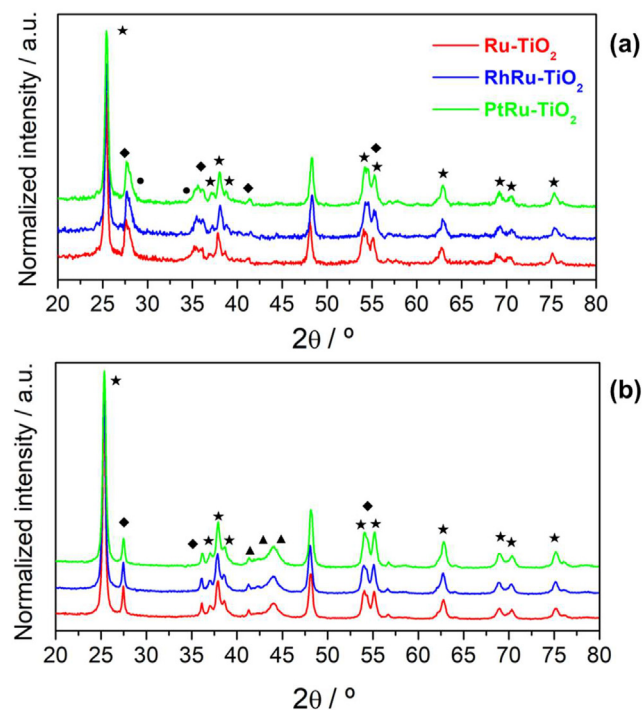
Fig. 1 – XRD patterns of (a) fresh and (b) reduced catalysts (★ TiO$_2$ anatase JCPDS 73-1764, ◆ TiO$_2$ Rutile JCPDS 78-1510, ● RuO$_2$ JCPDS 21-1172 and ▲ Ru JCPDS 6-0663).
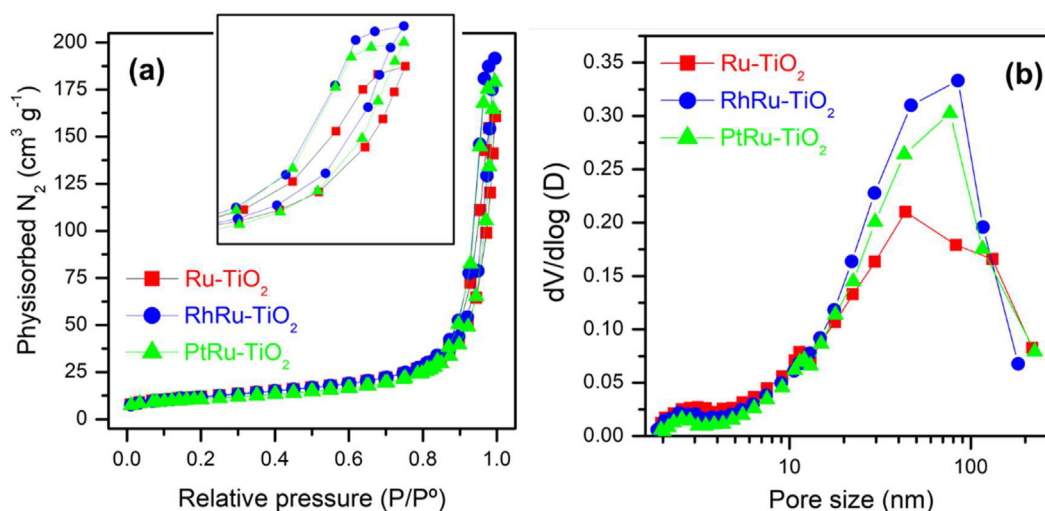
Fig. 2 – (a) Nitrogen adsorption isotherms obtained for Ru-based catalysts and (b) estimated pore size distribution by BJH model.

additional reduction zone at low temperature (<100 °C), mainly attributed to the so-called *spillover* effect promoted by those noble species. For instance, Kim et al. [35] reported the synthesis of 1 wt% Pt/TiO$_2$ calcined at several temperatures, obtaining in the reduction profile three reduction process at 100, 180 and 300 °C This agrees with the first reduction profile that can be observed in the PtRu–TiO$_2$ and RhRu–TiO$_2$ catalyst, which is attributed to well dispersed Pt species. Additionally, the RhRu–TiO$_2$ catalyst shows an extra reduction process at 500 °C. Wang and Ruckenstein reported the reduction of Rh in a 1% Rh coated MgO catalysts describing mainly two reduction processes, the first at 350 °C attributed to the reduction of MgRu$_2$O$_4$ species and the second one at 520 °C due to the reduction of Ru$_2$O$_3$ species [36]. However, the
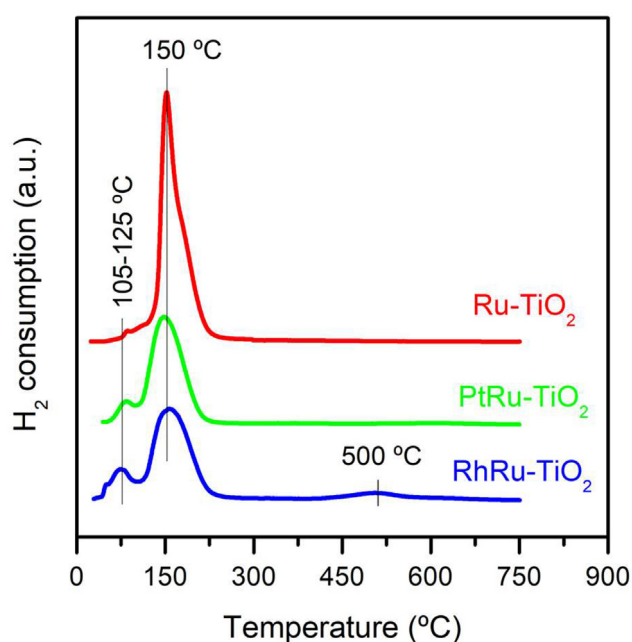
reduction process present in the RhRu–TiO$_2$ is shifted to slightly lower values likely due to the higher dispersion of the Rh$_2$O$_3$ species. Besides, in the noble metal on reducible supports TPR profiles, a reduction zone at 180 °C is frequently found and attributed to M-O$_v$-Ti^{3+} species related to strong metal-support interaction (SMSI) effect, being O$_v$ oxygen vacancies [37,38]. That is a common effect for Ru, Rh and Pt. All samples presented similar reducibility degree of about 100%.

Table 2 shows the metal dispersion calculated from H$_2$ chemisorption where is observed a slight decrease in the bimetallic catalyst, which may be attributed to the formation of bimetallic alloys, as was observed in above mentioned results. Komaya et al. reported the limitations of hydrogen chemisorption for the determination of the particle applied to a Ru/TiO$_2$ sample, where it was concluded that the dispersion could be overestimated due to a fraction of H$_2$ adsorbed that suffers spillover to the support. As a consequence, the number of active sites can be apparently higher. Additionally, if the sample is treated at high temperature reduction treatments, the metal could be partially encapsulated by the support, underestimating the mean particle size [39]. Table 2 also shows how the introduction of little Pt diminished the total amount of chemisorbed hydrogen to form a monolayer compared to the monometallic catalyst. Aguilar-Ríos et al. [40] obtained in their work similar results for Sn-modified Pt catalysts. After being doped with a ratio Sn/Pt < 1, the chemisorbed hydrogen increases. However, for Sn/Pt > 1 the H$_2$-monolayer value diminished. That may be explained in backbonding terms. In the monometallic Pt catalyst, the occupied

Fig. 3 – TPR-H$_2$ profiles for Ru–TiO$_2$, RhRu–TiO$_2$ and PtRu–TiO$_2$ catalysts.

Table 2 – Metal dispersion and metal particle size from H$_2$ chemisorption.

Sample	Monolayer (mmol H$_2$ g^{-1})	Dispersion (%)	Mean Particle Size (nm)
Ru–TiO$_2$	0.181	38.1	2.4
RhRu–TiO$_2$	0.184	36.0	2.5
PtRu–TiO$_2$	0.148	29.6	3.1

σ orbital of H_2 donates electronic density to the 6s Pt's orbital. For its part, the Pt donates electronic density from its $5d_{yz}$ to the antibonding σ orbital (back bonding), destabilizing and finally dissociating the bond. The addition of Sn produces a reduction of the electronic density transferred to the H_2 σ* orbital, diminishing the destabilization of the H−H and therefore making it less active. This explained the decrease in the H_2 chemisorbed when Sn/Pt > 1 but not the increase when the ratio is smaller than 1. Aguilar-Ríos et al. [40] also explained this suggesting that small amounts of Sn favours the Pt dispersion acting as anchoring sites for Pt due to the affinity that Pt has for Sn (and by extension every metal of Pt group - Ru, Rh, Pd, Os and Ir) according to theoretical calculations. However, according to these authors, despite the higher dispersion, every new created site must be less active.

Fig. 4 shows the TPD-H_2 profiles for the samples after chemisorption experiments in which an H_2 monolayer was firstly adsorbed. The two reduction processes observed are characteristics from transition metals and have been classified as H^*_w (weakly adsorbed hydrogen) and H^*_s (strongly adsorbed hydrogen). Sayari et al. [41] correlated a larger amount of H^*_w for particles between 0.9 and 2.2 nm, which is in good agreement with the present work for Ru and RhRu samples. This may be related to the fact that the H_2 adsorption/desorption is not dissociative, according to the work of Lin et al. where similar profiles were obtained [42]. By contrast, PtRu sample contains a large amount of H^*_s species and metallic particles are bigger than 2.2 nm (3.1 nm in as shown in Table 2). This suggest that Pt could favors the dissociative adsorption of H_2.

Surface analysis: XPS study

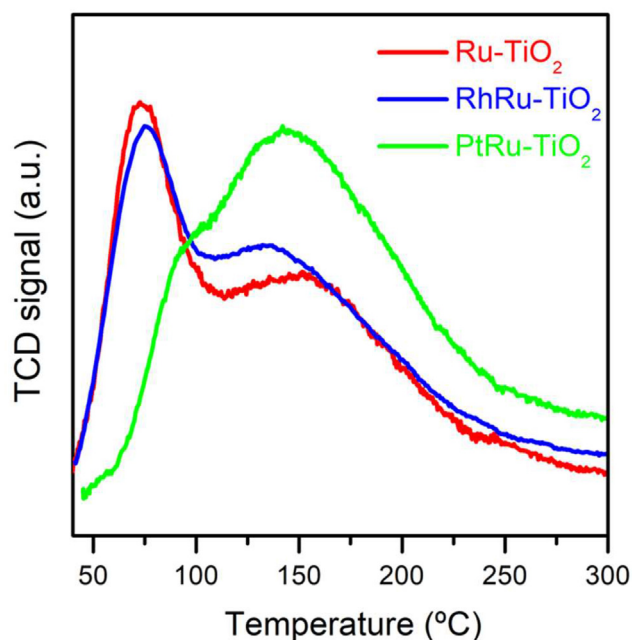To quantitatively and qualitatively analyze the surface species and their oxidation states before reaction, Ru, RhRu, and PtRu catalysts were *ex situ* reduced at 300 °C for 1 h in H_2 and characterized by XPS. Fig. 5 shows the Survey spectra of all the samples, where the peaks of the main elements, titanium, oxygen and carbon, are detected. As for the ruthenium peaks, the most intense are Ru3d, followed by Ru3p. Ru3p are very weak in which Ru3p3/2 is practically masked by the intense Ti2p3/2 peak. The Ru3d peaks are located in the C1s zone [43]. The surface composition is included in Table 3. Apparently, the surface chemical composition is similar in all the samples.

As can be expected, Fig. 6a shows that the O1s peak recorded at 530.3 eV is characteristic for oxides and is well suited with the peaks detected at 459.1 Ti 2p3/2 and 464.8 Ti 2p1/2 eV, with 2p doublet splitting of 5.7 eV, which is typical for TiO_2 (Fig. 6b) [43–45]. As seen in Fig. 6c, there is no peak at 461.2(3) eV for Ru 3p3/2 in any of the spectra of the three samples [45]. This could be related to the low surface concentration of ruthenium as also reflected in the Table 3 of surface composition. Ruthenium was detected in all catalysts by the peak at Ru 3d5/2 at 279.7 eV. As shown in Fig. 6c, the position of the peak is not affected by the incorporation of Rh or Pt. The regions Rh 3d and Pt 4f are also shown in Fig. 6d and e, respectively. From the position of the peaks for Ru 3d5/2 (279.7 eV) as well as for Rh 3d (307.3 eV with DS 4.7 eV) and for Pt 4f (70.2 eV with DS 3.4 eV), we can conclude that these are metallic species [44–46].

Catalytic performance

The catalysts were tested in selective CO methanation using two reaction gas compositions simulating a typical output
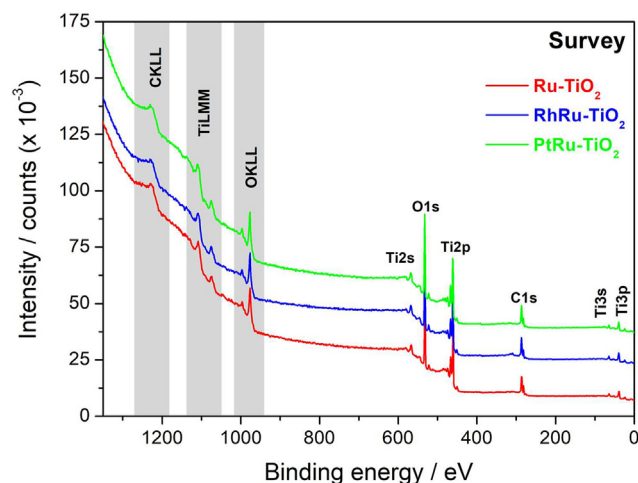
Fig. 5 − XPS Survey spectra for Ru−TiO_2, RhRu−TiO_2 and PtRu−TiO_2 catalysts.

Fig. 4 − TPD-H_2 profiles for Ru−TiO_2, RhRu−TiO_2 and PtRu−TiO_2 catalysts.

Table 3 − Surface composition determined by X-ray Photoelectron Spectroscopy (XPS analysis).

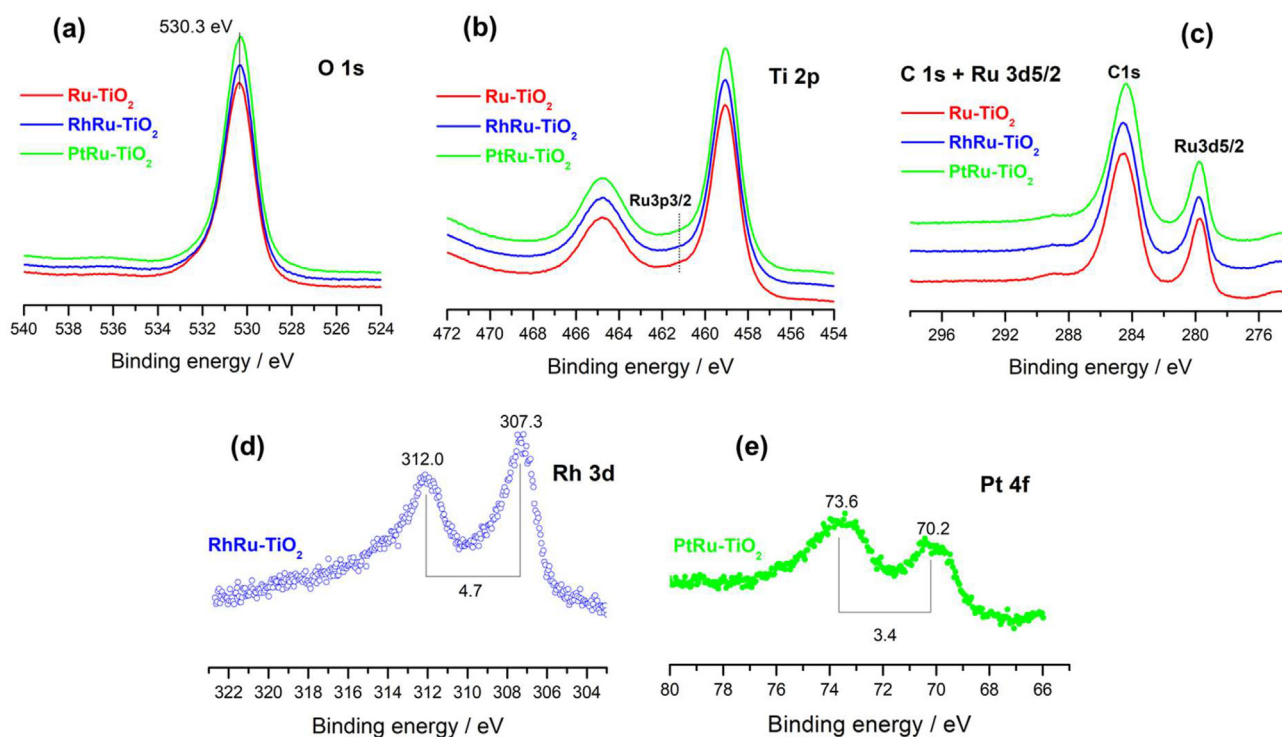| Catalysts	Surface content (at. %)					
	Ti2p + Ru3p3/2	O1s	C1s + Ru3d3/2	Ru3d5/2	Rh3d	Pt4f
Ru−TiO_2	18.9	45.3	34.4	1.4		
RhRu−TiO_2	19.5	45.8	32.9	1.2	0.6	
PtRu−TiO_2	19.5	46.0	33.0	1.3		0.2

Fig. 6 – High-resolution XPS spectra for O 1s (a), Ti 2p (b), C 1s + Ru 3d5/2 (c), Rh 3d (d) and Pt 4f (e) collected on Ru–TiO$_2$, RhRu–TiO$_2$ and PtRu–TiO$_2$ catalysts.

stream of a water-gas shift (WGS) unit: H$_2$ (50 vol%), CO$_2$ (15 vol %), H$_2$O (15 vol%) and CO (1 vol% or 300 ppm) balanced with N$_2$. Fig. 7 shows the performance in terms of CO and CO$_2$ conversion and CO methanation selectivity as a function of reaction temperature for all the catalysts when the reaction was performed with 1 vol% of CO inlet. As can be noticed, increasing the temperature leads to an exponential growth of CO conversion between 200 and 240 °C (Fig. 7a). Meanwhile,

Fig. 7b shows that CO$_2$ conversion was initiated at about 220 °C and increasing the temperature above 260 °C a drop in CO conversion become simultaneously evidenced (Fig. 7a inlet). This negative CO conversion as temperature was increased suggests that CO is produced in parallel via reverse water gas shift (RWGS) reaction. Consequently, CO methanation is thermodynamically unfavorable at higher temperatures (Fig. 7c) and the effluent CO concentration is increased with
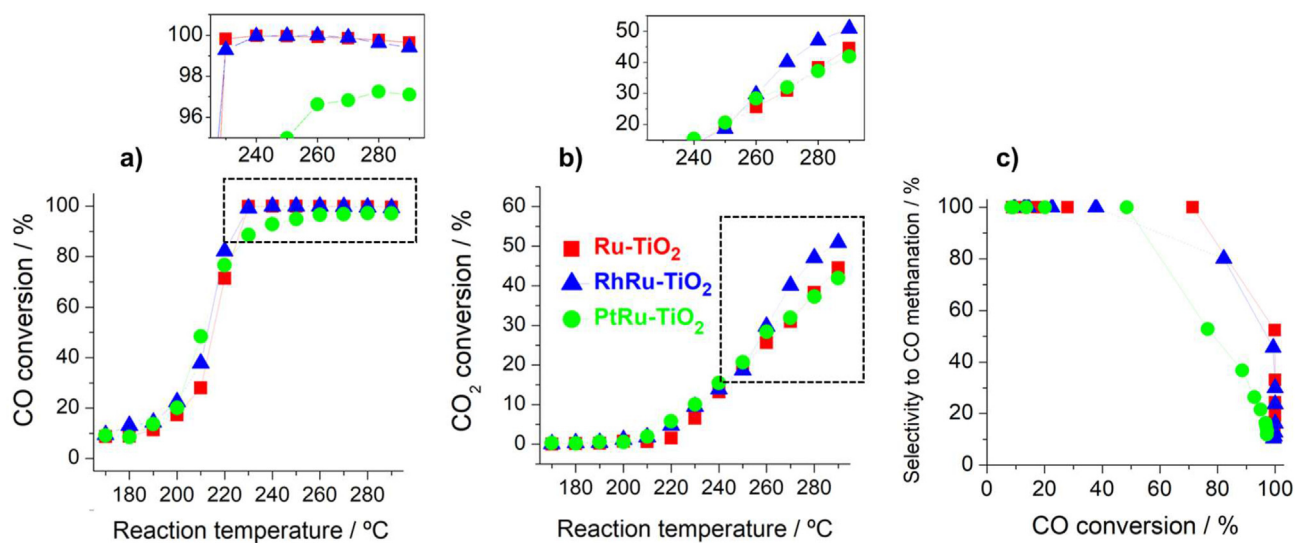

Fig. 7 – CO and CO$_2$ conversion versus temperature (a and b, respectively) and selectivity to CO methanation against CO conversion (c) for Ru/TiO$_2$, RhRu/TiO$_2$ and PtRu/TiO$_2$ samples. Reaction conditions: [Space velocity: WHSV = 80 L g^{-1} h^{-1}; CO concentration: 1 vol%; H$_2$ vol% = 50; CO$_2$ vol% = 15; H$_2$O vol% = 15].

increasing temperature. Although the three catalysts presented similar activity, it can be noticed that PtRu catalyst shows minor CO conversion at high temperature (Fig. 7a inlet). Furthermore, Fig. 7c clearly shows that Pt addition affects negatively the selectivity of CO methanation. According to Xu et al. [47], the reason for this low CH_4 production in PtRu catalyst can be related to the alloy formation that prevents the C−O bond cleavage of and subsequent hydrogenation of C to CH_4. This argument is coherent with our results of characterization discussed above. On the other hand, it is also significant in Fig. 7b inlet that Rh addition increases slightly the CO_2 conversion although selectivity of CO methanation is hardly affected. This indicates that Rh favors CO_2 methanation against reverse water gas shift. It is well known that Rh is an excellent active metal for CO_2 methanation [48].

Subsequently and without reactivation, the catalysts were tested in the same conditions but with a lower concentration of CO (300 ppm) balanced with N_2. As shown in Fig. 8, the effect of the metal doping only is positive in the case of Rh doped catalyst, which increases the catalytic activity and selectivity in the whole temperature range. Similarly for the three samples, CO methanation was initiated at relatively low temperatures achieving conversion about 70% at 130 °C and increasing with temperature until completed CO conversion. On the other side, the CO_2 methanation initiates once the CO conversion has reached approximately the 90% in every case. It is noteworthy that CO conversion decreases at higher temperatures due to the RWGS contribution, which tend to produce CO from CO_2 and hydrogen, and which is highly visible in PtRu but not appreciated in the Rh doped one.

It has been tested that polymer-electrolyte-membranes fuel cells (PEMFCs) only tolerates H_2 stream with CO concentration below 20 ppm. Considering that inlet steam contains 300 ppm of CO, a minimum conversion of 93% will be required to decrease the concentration below 20 ppm in the outlet stream. In order to compare the three catalysts, we have defined T_{93} as the required temperature to achieve CO

conversion of 93%. Remarkably, Fig. 8 inlet shows that RuRh bimetallic catalyst decreases the temperature T_{93} of selective CO methanation in absence of CO_2 methanation. In comparison to monometallic Ru and bimetallic PtRu, this variation decrease the total consumption of hydrogen and it could become important in industrial-volume streams.

Conclusions

In this work, a Ru supported on TiO_2 catalyst was doped with Rh and Pt by wet impregnation method and tested in CO selective methanation using two simulated mixtures from reforming reactors. The obtained catalytic results showed that with a lower concentration of CO (300 ppm) the addition of Rh as dopant results to be advantageous in the methanation catalyst while that Pt has a negative effect since it promotes the reverse water gas shift reaction decreasing the selectivity of methanation. At higher concentration values of CO (1 vol%), Pt addition is also detrimental for CO selective methanation whereas that Ru and RuRh catalysts are practically identical. Although the positive effect of Rh observed at low CO concentrations is relatively mild and may not compensate for its use in this particular case due to the expensive nature of this metal, this approach takes one step further for a better understanding of the promotion effect of other noble metals in a Ru methanation catalyst.

Declaration of competing interest

The authors declare that they have no known competing financial interests or personal relationships that could have appeared to influence the work reported in this paper.

Acknowledgments

Fig. 8 – CO and CO_2 conversion versus temperature for Ru/TiO_2, RhRu/TiO_2 and PtRu/TiO_2 samples. Reaction conditions: [Space velocity: WHSV = 80 L g^{-1} h^{-1}; CO concentration: 300 ppm; H_2 vol% = 50; CO_2 vol% = 15; H_2O vol% = 15].

REFERENCES

[1] Krumpelt M, Krause TR, Carter JD, Kopasz JP, Ahmed S. Fuel processing for fuel cell systems in transportation and portable power applications. Catal Today 2002;77:3–16.

[2] Pei P, Wang M, Chen D, Ren P, Zhang L. Key technologies for polymer electrolyte membrane fuel cell systems fueled impure hydrogen. Prog Nat Sci Mater Int 2020;30:751–63.

[3] Wang Y, Chen KS, Mishler J, Cho SC, Adroher XC. A review of polymer electrolyte membrane fuel cells: technology, applications, and needs on fundamental research. Appl Energy 2011;88:981–1007.

[4] Postole G, Auroux A. The poisoning level of Pt/C catalysts used in PEM fuel cells by the hydrogen feed gas impurities: the bonding strength. Int J Hydrogen Energy 2011;36:6817–25.

[5] Minutillo M, Perna A. Behaviour modelling of a PEMFC operating on diluted hydrogen feed. Int J Energy Res 2008;32:1297–308.
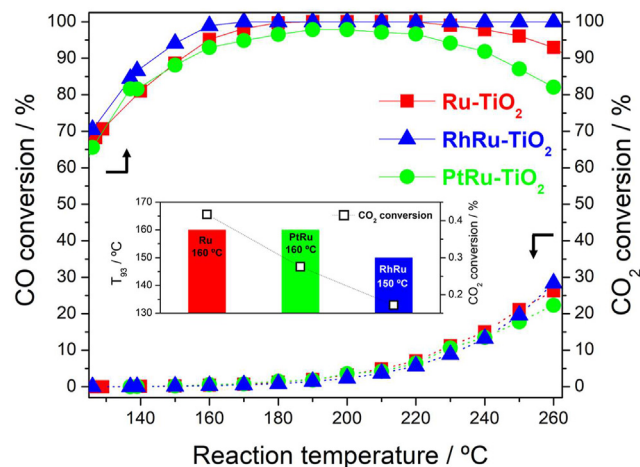
[6] Dagle RA, Wang Y, Xia G-G, Strohm JJ, Holladay J, Palo DR. Selective CO methanation catalysts for fuel processing applications. Appl Catal Gen 2007;326:213–8.

[7] Görke O, Pfeifer P, Schubert K. Highly selective methanation by the use of a microchannel reactor. Catal Today 2005;110:132–9.

[8] Panagiotopoulou P, Kondarides DI, Verykios XE. Selective methanation of CO over supported Ru catalysts. Appl Catal B Environ 2009;88:470–8.

[9] Alihosseinzadeh A, Nematollahi B, Rezaei M, Lay EN. CO methanation over Ni catalysts supported on high surface area mesoporous nanocrystalline γ-Al_2O_3 for CO removal in H_2-rich stream. Int J Hydrogen Energy 2015;40:1809–19.

[10] Battulga B-U, Bold T, Byambajav E. Effect of Fe and Co promoters on CO methanation activity of nickel catalyst prepared by impregnation – co-precipitation method. Int J Chem React Eng 2020;18.

[11] Tada S, Kikuchi R. Mechanistic study and catalyst development for selective carbon monoxide methanation. Catal Sci Technol 2015;5:3061–70.

[12] Nematollahi B, Rezaei M, Lay EN. Selective methanation of carbon monoxide in hydrogen rich stream over Ni/CeO2 nanocatalysts. J Rare Earths 2015;33:619–28.

[13] Nematollahi B, Rezaei M, Amini E, Nemati Lay E. Preparation of high surface area $Ni/MgAl_2O_4$ nanocatalysts for CO selective methanation. Int J Hydrogen Energy 2018;43:772–80.

[14] Ishihara T, Harada K, Eguchi K, Arai H. Electronic interaction between supports and ruthenium catalysts for the hydrogenation of carbon monoxide. J Catal 1992;136:161–9.

[15] Yamaguchi T, Morita T, Salama TM, Tanabe K. Surface properties of ZrO_2 dispersed on SiO_2. Catal Lett 1990;4:1–6.

[16] Takenaka S, Shimizu T, Otsuka K. Complete removal of carbon monoxide in hydrogen-rich gas stream through methanation over supported metal catalysts. Int J Hydrogen Energy 2004;29:1065–73.

[17] Kim YH, Park ED, Lee HC, Lee D. Selective CO removal in a H_2-rich stream over supported Ru catalysts for the polymer electrolyte membrane fuel cell (PEMFC). Appl Catal Gen 2009;366:363–9.

[18] Gallezot P, Richard D. Selective hydrogenation of α,β-unsaturated aldehydes. Catal Rev 1998;40:81–126.

[19] Sakakini BH. Temperature-programmed surface reaction (TPSR) of pre-adsorbed carbon CO and COH_2 synthesis over Ru-$CsAl_2O_3$ catalysts. J Mol Catal Chem 1997;127:203–9.

[20] Solymosi F, Erdöhelyi A, Kocsis M. Methanation of CO_2 on supported Ru catalysts. J Chem Soc Faraday Trans 1 Phys Chem Condens Phases 1981;77:1003–12.

[21] Dey S, Dhal GC. Applications of rhodium and ruthenium catalysts for CO oxidation: an overview. Polytechnica 2020;3:26–42.

[22] Zhang S, Ji W, Feng N, Lan L, Li Y, Ma Y. Study on Rh(I)/Ru(III) bimetallic catalyst catalyzed carbonylation of methanol to aceticacid. Materials 2020;13.

[23] Shao Y, Yin G, Gao Y. Understanding and approaches for the durability issues of Pt-based catalysts for PEM fuel cell. J Power Sources 2007;171:558–66.

[24] Sreedhar I, Varun Y, Singh SA, Venugopal A, Reddy BM. Developmental trends in CO_2 methanation using various catalysts. Catal Sci Technol 2019;9:4478–504.

[25] Martínez Tejada LM, Muñoz A, Centeno MA, Odriozola JA. *In-situ* Raman spectroscopy study of Ru/TiO$_2$ catalyst in the selective methanation of CO. J Raman Spectrosc 2016;47:189–97.

[26] González-Castaño M, Ivanova S, Laguna OH, Martínez T LM, Centeno MA, Odriozola JA. Structuring Pt/CeO$_2$/Al$_2$O$_3$ WGS catalyst: introduction of buffer layer. Appl Catal B Environ 2017;200:420–7.

[27] Jurado L, García-Moncada N, Bobadilla LF, Romero-Sarria F, Odriozola JA. Elucidation of water promoter effect of proton conductor in WGS reaction over Pt-based catalyst: an *operando* DRIFTS study. Catalysts 2020:10.

[28] Shen X, Garces L-J, Ding Y, Laubernds K, Zerger RP, Aindow M, Neth EJ, Suib SL. Behavior of H_2 chemisorption on Ru/TiO_2 surface and its application in evaluation of Ru particle sizes compared with TEM and XRD analyses. Appl Catal Gen 2008;335:187–95.

[29] Goodwin JG. Characterization of highly dispersed Ru catalysts by chemisorption. J Catal 1981;68:227–32.

[30] Álvarez Moreno A, Ramirez-Reina T, Ivanova S, Roger A-C, Centeno MÁ, Odriozola JA. Bimetallic Ni–Ru and Ni–Re catalysts for dry reforming of methane: understanding the synergies of the selected promoters. Front Chem 2021;9.

[31] Thommes M, Kaneko K, Neimark AV, Olivier JP, Rodriguez-Reinoso F, Rouquerol J, Sing KSW. Physisorption of gases, with special reference to the evaluation of surface area and pore size distribution (IUPAC Technical Report). Pure Appl Chem 2015;87:1051–69.

[32] Zhao Z, Zhang L, Tan Q, Yang F, Faria J, Resasco D. Synergistic bimetallic Ru–Pt catalysts for the low-temperature aqueous phase reforming of ethanol. AIChE J 2019;65:151–60.

[33] Abdel-Mageed AM, Wiese K, Parlinska-Wojtan M, Rabeah J, Brückner A, Behm RJ. Encapsulation of Ru nanoparticles: modifying the reactivity toward CO and CO_2 methanation on highly active Ru/TiO_2 catalysts. Appl Catal B Environ 2020;270:118846.

[34] Corradini SAdS, Lenzi GG, Lenzi MK, Soares CMF, Santos OAA. Characterization and hydrogenation of methyl oleate over Ru/TiO$_2$, Ru–Sn/TiO catalysts. J Non-Cryst Solids 2008;354:4865–70.

[35] Kim SS, Park KH, Hong SC. A study of the selectivity of the reverse water–gas-shift reaction over Pt/TiO$_2$ catalysts. Fuel Process Technol 2013;108:47–54.

[36] Wang HY, Ruckenstein E. Partial oxidation of methane to synthesis gas over MgO- and SiO$_2$-supported rhodium catalysts. J Catal 1999;186:181–7.

[37] Oi LE, Choo M-Y, Lee HV, Ong HC, Hamid SBA, Juan JC. Recent advances of titanium dioxide (TiO$_2$) for green organic synthesis. RSC Adv 2016;6:108741–54.

[38] Bertella F, Concepción P, Martínez A. TiO$_2$ polymorph dependent SMSI effect in Co-Ru/TiO$_2$ catalysts and its relevance to Fischer-Tropsch synthesis, Catal. Today Off 2017;289:181–91.

[39] Komaya T, Bell AT, Wengsieh Z, Gronsky R, Engelke F, King TS, Pruski M. The influence of metal-support interactions on the accurate determination of Ru dispersion for Ru/TiO$_2$. J Catal 1994;149:142–8.

[40] Aguilar-Ríos G, Valenzuela M, Salas P, Armendáriz H, Bosch P, Del Toro G, Silva R, Bertín V, Castillo S, Ramírez-Solís A, Schifter I. Hydrogen interactions and catalytic properties of platinum-tin supported on zinc aluminate. Appl Catal Gen 1995;127:65–75.

[41] Sayari A, Wang HT, Goodwin JG. Surface structure dependence of reversible/weak H_2 chemisorption on supported Ru. J Catal 1985;93:368–74.

[42] Lin H-Y, Chen Y-W. The kinetics of H_2 adsorption on supported ruthenium catalysts. Thermochim Acta 2004;419:283–90.

[43] https://www.thermofisher.com/es/es/home.html.

[44] http://www.xpsfitting.com.

[45] https://srdata.nist.gov/xps/.

[46] http://www.lasurface.com/accueil/.

[47] Xu W, Si R, Senanayake SD, Llorca J, Idriss H, Stacchiola D, Hanson JC, Rodriguez JA. *In situ* studies of CeO$_2$-supported Pt, Ru, and Pt—Ru alloy catalysts for the water—gas shift reaction: active phases and reaction intermediates. J Catal 2012;291:117—26.

[48] Karelovic A, Ruiz P. Mechanistic study of low temperature CO$_2$ methanation over Rh/TiO$_2$ catalysts. J Catal 2013;301:141—53.